The Growth of Ice Crystals by Molecular Diffusion

HYUN YOUK, ROLAND LIST, AND THEOPHILUS OLA

Department of Physics, University of Toronto, Toronto, Ontario, Canada

ABSTRACT

The mass transfer of water molecules by diffusion onto ice particles is best described by their Sherwood number (Sh), a dimensionless quantity, which combines molecular and convective effects and depends on the airflow as represented by the Reynolds number (Re). While Sh (Re > 0) has been previously measured in experiments for typical crystal shapes, the limiting case of pure molecular diffusion (Sh_0) for zero flow with Re = 0 is not known well and needs independent determination.

The direct numerical solution of the controlling Laplace equation links diffusion with electric fields through the electrostatic analogy. It will be solved for the electrostatic potential V around a crystal-shaped conductor of capacitance C. The results will then be converted by similarity theory. This led to the first numerical determination of Sh_0 for hexagonal plates, hexagonal columns, stellar crystals, capped columns, and broad-branched crystals. The new data represent another necessary step in the formulation of an experiment-based theory of the growth of freely falling ice crystals in the atmosphere.

A discrete version of Gauss's flux law is developed to compute the flux generated by a crystal-shaped conductor in a finite Cartesian grid box, using a Gauss–Seidel iterative scheme. This method is general and can be applied to compute Sh_0 for any rectilinear shapes to any degree of accuracy. The dimensionless mass transfer by molecular diffusion, Sh_0, is identical to the diffusion of heat characterized by the Nusselt number Nu_0.

1. Introduction

The growth of an atmospheric ice crystal is determined by its heat and mass transfer. They are characterized by dimensionless numbers, the Nusselt number (Nu) for heat and the Sherwood number (Sh) for mass transfer. Both numbers are functions of the airflow as described by the dimensionless Reynolds number ($Re = vD\rho\eta^{-1}$), where v is the relative air velocity, D the diameter, ρ is the density of the fluid (air), and η the dynamic viscosity of the fluid). For pure molecular diffusion Sh_0 (Re = 0) and Nu_0 are identical. In this study Sh_0 was explored. Here, Sh is an expression of mass conservation, stating that what evaporates at the surface is diffused away through the air, whereas Sh_o expresses the mass transfer by molecular diffusion only with $Sh_0 = \beta D D_{wa}^{-1}$, where β is the mass transfer per unit of particle surface and time, D its diameter, and D_{wa} the diffusivity of water vapor in air. The quantities to be used when calculating the mass transfer are either Sh or Sh_0. A note of caution: The characteristic length to be used in all similarity numbers has to be consistent, it is either the diameter, the radius, or a specially defined length (Pasternak and Gauvin 1960). The use of ventilation coefficients is discouraged because they do not automatically include the effects of pressure. References to values of $Sh_0 = 2$ for spheres indicate that the characteristic length is the diameter. Using the radius would produce $Sh_0 = 1$.

The general forms of Sh and Nu always contain a molecular diffusion component (Schemenauer 1972). The convective effects are considered additive and may control larger, faster falling particles. For a 1-mm hexagonal plate at an appropriate cloud temperature and height the molecular part is reduced to ~40% of the total diffusion (List and Schemenauer 1971). For the other shapes it is higher. The functional dependence of Sh on Re has been directly measured by Schemenauer and List (1978) for specific crystal shapes, but not their anchoring points representing molecular diffusion alone (at Re = 0).

Historically, there have been two main methods of approaching either Sh_0 or Nu_0. In a first investigation,

Corresponding author address: Prof. Roland List, Dept. of Physics, University of Toronto, 60 St. George Street, Toronto, ON M5S 1A7, Canada.
E-mail: list@atmosp.physics.utoronto.ca

experimental data on the axial growth rates were fitted to empirical equations (Todd 1964; Beard and Pruppacher 1971). This method involves many assumptions and extrapolations and is not considered reliable according to Jayaweera (1971). Well founded, however, is the "electrostatic analogy" between the electrical field divergence of a charged conductor particle and the molecular diffusion of mass (water molecules) from a geometrically similar crystal to its environment. Both are governed by the Laplace equation. Similarity theory will provide the link between the two systems.

Houghton (1950) estimated Sh_0 by treating crystal shapes as limiting cases of shapes whose exact Sh_0 values were known. He used a flat disc to approximate thin plates and dendrites, while a sphere was stretched to a prolate spheroid to approximate ice needles. In a second approach to the electrostatic analogy, McDonald (1963) directly measured the capacitance of crystal-shaped (rectilinear) particles in a Faraday cage and compared them with that of a known sphere. The effect of the electrical wire, necessary for measurement and suspension, turned out to lower Sh_0 by ~20%–50%. However, assuming that the same correction factor for spheres would also apply to any crystal shape led McDonald to tentatively corrected values for Sh_0 for those shapes—with limited success.

Before embarking on a numerical solution to the diffusion equation, the authors have considered applying a general electrochemical method (Schuepp and List 1969) to solve for the molecular diffusion. However free convection would have affected the results and explorations of the Grashof similarity number did not seem to simplify the problem. Thus, the direct numerical approach was chosen.

The solutions by the electrostatic analogy are important to cloud physics where they apply to the first stages of the formation of precipitation. They have potential for other types of ice crystals, such as bullets and rosettes, as they are occurring in cirrus clouds. These two types are relevant to satellite measurements and climate change modeling. Rosette crystals occurring in cirrus clouds have already been treated by Chiruta and Wang (2003) with the help of a numerical procedure different from ours.

Including free fall at Re ≠ 0, Sh would normally be expressed by $Sh = Sh_0 + k_{Sh} Sc^{1/3} Re^{1/2}$, with the equivalent for heat transfer given by $Nu = Nu_0 + k_{Nu} Pr^{1/3} Re^{1/2}$, where k_i is a constant, Sc is the Schmidt number, and Pr the Prandtl number. Combined equations for molecular diffusion and the added convective diffusion have been measured by Schemenauer and List (1978) for shapes very similar to the ones explored in the present study. However, an extension of the present study to account for free fall is subject to additional investigations addressing also particle oscillation (as expressed by the Strouhal number) and its effect on free fall and the heat and mass transfer. These complications led to the limitation of this paper to molecular diffusion as experienced by crystals.

Thus, the purpose of this study is

(a) To develop a general method to numerically calculate the molecular mass transfer by diffusion; that is, the Sherwood numbers at zero flow ($Sh_0 \equiv Nu_0$) for ice crystals;
(b) to describe the crystal shapes appropriate for the numerical scheme to formulate a discrete version of the Gauss flux law;
(c) to apply the method and calculate Sh_0 ($\equiv Nu_0$) for specific crystals;
(d) to discuss the results and address issues to be resolved in the future.

2. Electrostatic analogy

Like the standard in the field of heat and mass transfer, the electrostatic analogy relies on the assumption that both temperature and saturation vapor pressure over the surface of an ice crystal are constant in a steady-state diffusive vapor field. Both this field and the electrostatic potential in a vacuum obey Laplace's equation with analogous boundary conditions, as required by geometric similarity. In this analogy, Sh_0 is related to the capacitance of the crystal by

$$Sh_0 = \frac{4\pi CL}{A},\qquad(1)$$

where A is the surface area, L is the characteristic length such as the radius of the circumscribing circle or half the height of the hexagonal prism, and C is the capacitance in electrostatic units. In these units, the capacitance C has the dimension of length, which will make Sh_0 dimensionless. For a sphere where $C = R$, the radius, $Sh_0 = 2$ by definition. For the complex crystals additional characteristics, such as aspect ratios, need to be defined

3. Application of the Gauss–Seidel method

a. Derivation of the Gauss–Seidel method

The Gauss–Seidel (or Jacobi's) iterative scheme is used to solve the Laplace equation system by finding the capacitance C of a conductor. It is applied to crystals with rectilinear shapes in a Cartesian grid system. Rectilinear shapes are those that can be constructed with a finite number of straight edges. Discs and
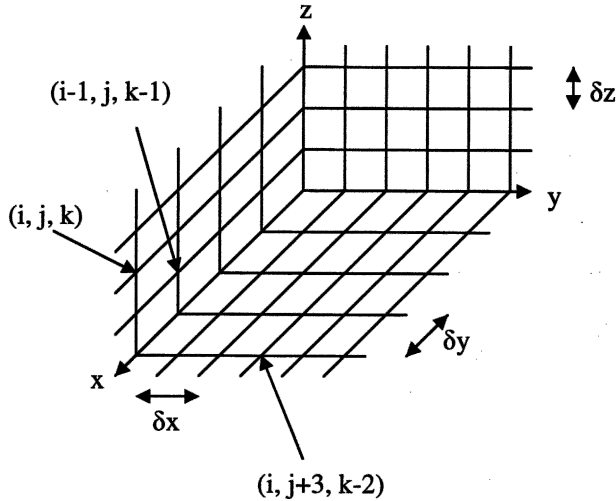
FIG. 1. The $200 \times 200 \times 200$ Cartesian grid box with variable lattice separations δx, δy, and δz. Each lattice point is labeled by a positive index (i, j, k) with $(1, 1, 1)$ being the origin.

spheres are better treated in finite polar coordinate systems.

A Cartesian grid system (lattice) with $200 \times 200 \times 200$ lattice points is used to represent a Faraday cage with a conductive wall and a potential $V = 0$. The crystal is freely suspended at the center of this cage with a constant potential at its surface. Each lattice point is labeled by positive integer indices (i, j, k), where i, j, and k run along the x axis, y axis, and z axis respectively. To simplify the analysis, a parameter μ is introduced, where μ can be either x, y, or z. Thus $\hat{\mu}$ represents the unit vector along the μ axis; $\delta\mu$ represents the separation length between two adjacent points along the μ direction (Fig. 1). Assuming that the grid points are sufficiently close to each other, the partial derivative of potential V at point (i, j, k) [denoted $V(i, j, k)$] can be approximated by the following first-order finite difference equation

$$\frac{\partial V(i, j, k)}{\partial \mu} \equiv \frac{V[(i, j, k) + \hat{\mu}] - V(i, j, k)}{\delta\mu}. \quad (3)$$

Furthermore, defining a function $A(\mu)$ as

$$A(\mu) \equiv V[(i, j, k) + \hat{\mu}] + V[(i, j, k) - \hat{\mu}], \quad (4)$$

the finite difference approximation of second-order partial derivatives of V can be approximated to first order by

$$\frac{\partial^2 V(i, j, k)}{\partial \mu^2} = \frac{A(\mu) - 2V(i, j, k)}{2(\delta\mu)^2}. \quad (5)$$

To further simplify the analysis, the following proportionality constants are introduced:

$$\alpha \equiv \left(\frac{\delta y}{\delta x}\right)^2$$

$$\beta \equiv \left(\frac{\delta z}{\delta x}\right)^2. \quad (6)$$

The Laplace equation in the discrete Cartesian grid system then becomes

$$0 \approx \frac{B(x)}{2(\delta x)^2} + \frac{B(y)}{2\alpha(\delta x)^2} + \frac{B(z)}{2\beta(\delta x)^2}, \quad (7)$$

where $B(\mu) \equiv A(\mu) - 2V(i, j, k)$. Rearranging of (7) gives the final desired form of the potential

$$V(i, j, k) = \frac{\alpha\beta A(x) + \beta A(y) + \alpha A(z)}{2(\alpha\beta + \alpha + \beta)}. \quad (8)$$

An iterative scheme that uses the centered difference Eq. (8) is

$$V_{n+1}(i, j, k) = \frac{\alpha\beta A_n(x) + \beta A_n(y) + \alpha A_n(z)}{2(\alpha\beta + \beta + \alpha)}, \quad (9)$$

where the subscript n indicates the value of the variable in question at the nth iteration. This is the equation used by the Gauss–Seidel iterative scheme for solving Laplace's equation.

b. Convergence rate

To make use of Gauss–Seidel scheme, Dirichlet boundary conditions are specified; V is set zero on the edges of the $200 \times 200 \times 200$ grid box while it is assigned to an arbitrarily chosen constant V_0 on the faces of the crystal. On all other lattice points, V is initially set to zero. Then $V(i, j, k)$ is computed via (9) layer by layer, starting with the $k = 1$ layer, then moving up to $k = 200$ layer. The center of crystal is at $k = 100$ layer, at the center of the grid box. One iteration is completed when $V(i, j, k)$ has been computed for all points in the grid box. This procedure is repeated. A measure of settling of the potential at a point (i, j, k) is defined as $\delta V(i, j, k) = |V_n(i, j, k) - V_{n-1}(i, j, k)|$. The iteration is halted when the following convergence criterion, summed over all grid points, is met:

$$\sum_{(i,j,k)} \delta V(i, j, k) < \varepsilon, \quad (10)$$

where ε is desired precision of the computation. The number of iterations r required to reduce the overall error by a factor of 10^{-p} is

$$r \sim O(pN^3), \quad (11)$$

where N is the number of grid points in an $N \times N \times N$ cubic regular Cartesian grid system.

An important question to ask at this junction is if the

scheme presented above guarantees convergence to the exact solution. Laplace's equation possesses the well known maximum value property and the mean value property. It can be shown that the solution derived by (9) also obeys these properties (Strauss 1992, 208–210). Then by the same way one shows that the solution to Laplace's equation is unique and that the solution derived by (9) is unique. The reader is referred to the literature on numerical methods for a proof that (9) always converges to the exact solution.

To test if the outer faces of the $200 \times 200 \times 200$ grid box are sufficiently far away from the conductor suspended in the middle, Laplace equation was solved for $150 \times 150 \times 150$ grid box and the values of potential obtained were compared to those from the $200 \times 200 \times 200$ grid box. Floating point numbers with a precision of ten decimal places were used in finding the potential V at every grid point within the box. Maintaining the same values of α and β for a given crystal, the Laplace equation was solved in both grid boxes. By looking at the value of V at point (i, j, k) in $150 \times 150 \times 150$ box and the V at the corresponding point (i, j, k) in $200 \times 200 \times 200$ box, and doing this for all the points lying within 1 to 20 grid spaces away from the faces of the crystal, it was found that the two sets of values of V differed by at most 10^{-7} in this region. For grid points within one and six spaces away from the crystal faces, it was found that the difference was at most 10^{-9}. This showed that within this 10-digit precision, the walls of a $200 \times 200 \times 200$ Faraday cage were far enough from the faces of the crystal, and thus could be effectively considered to be infinitely far away from the crystal. This justifies setting the potential to be 0 on the walls of the Faraday cage.

There are other computational methods than Gauss–Seidel scheme to solve the Laplace's equation numerically, such as the simultaneous overrelaxation (SOR) method. The SOR method has a convergence rate of $O(N^2)$ for a $N \times N \times N$ Cartesian system. Nevertheless, the Gauss–Seidel method was chosen since it is simple and can be easily implemented. The SOR method also requires a nontrivial task of choosing the initial value of a parameter known as the relaxation coefficient. The results one obtains from SOR are dependent on which initial value was chosen, making implementation of SOR more nontrivial than Gauss–Seidel.

4. Representing shapes on finite lattice

a. Hexagonal plate

All the ice crystal shapes have been modeled using a Cartesian grid box with variable lattice separations. A
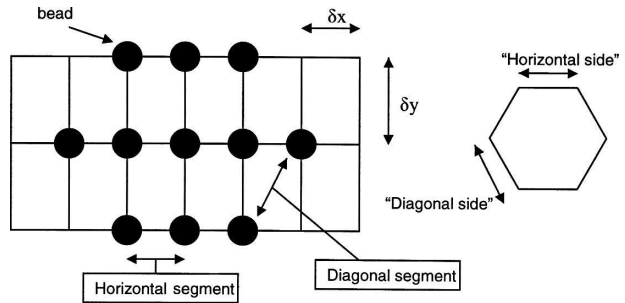

FIG. 2. Optimal representation of hexagon on the grid system with $2N_d = N_h$, where N_d and N_h represent the number of diagonal and horizontal segments respectively, with $N_d = 1$. Grid with bead represents part of the hexagon. Shape simplified, ratio diagonal length to horizontal sides 0.87, angles correct.

finite number of points need to be established to represent each shape and to determine the optimal proportionality factors α and β (6).

The important features of a hexagonal plate are its vertices. A regular ($\alpha = \beta$) Cartesian grid however does not accommodate this shape. However, $\alpha = 3$ allows for a construction of a hexagon with all its vertices lying on the grid points, but with the diagonal sides different by a factor of 0.87 from the horizontal sides (see Fig. 2). For the purpose of this paper, this difference was treated acceptable and higher resolutions were not attempted to reduce the difference closer to zero. In the calculations, the properties of the plate were based on the ideal length. Here, $\beta < 1$ would mean that the floor and ceiling of the grid box are closer to the crystal than the other sides. This is not desired since one would like the sides to be as far away from the crystal as possible to represent the boundary at infinity where the electrostatic potential vanishes. In addition $\beta \ll 1$ is not appropriate since this reduces the accuracy of the calculations. Thus $\beta = 1$ is chosen. Further, the plate is assumed to be infinitesimally thin and lying on a single xy planar layer of lattice points. The plate, like all other shapes mentioned in this paper, is centered in the grid box. This optimal representation of the hexagonal plate results in the relationship: $N_d = N_h/2$, where N_d and N_h are the number of segments used to represent a diagonal and the horizontal sides of the hexagon, respectively (Fig. 2). The input data for the hexagonal plate are displayed in Table 1, together with all the data of the other shapes. Note that the radius of the circumscribing circle or hexagon side length is $8\delta x$, with a surface area described by A.

b. Hexagonal column

Once the hexagonal plate (HP) is modeled, the hexagonal column (HC) requires very little work. The col-

TABLE 1. Dimensions of HP, HC, BB dendrites, SC, and CC in terms of multiples of an arbitrary length unit δx, with surface areas A, column heights and aspect ratios (where required), with the numerical results for capacitance C, and $Sh_0 \equiv Nu_0$. Here, R is the radius of the circumscribing circle for HP, BB, and SC, and the prism cross sections of HC and CC; L is half the height for HC and CC. The aspect ratio of the columns is the ratio of column height to R. Note that the thickness of HP, BB, and SC is assumed to be negligible compared to the top and bottom surfaces.

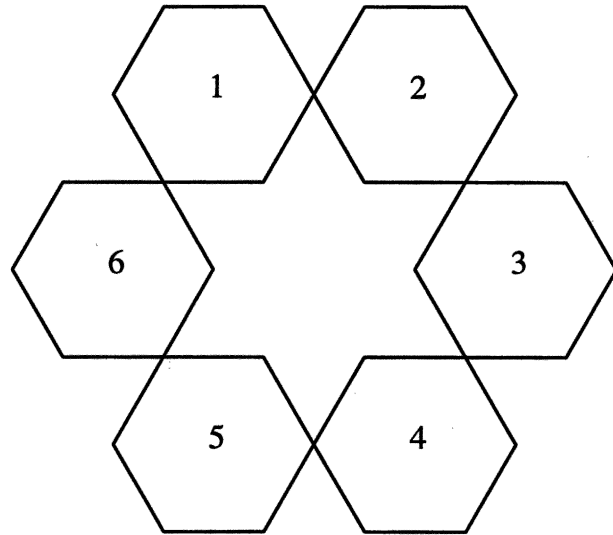| Shape	Dimensions used	C	$Sh_0 \equiv Nu_0$
HP	$R = L = 8(\delta x)$ $A = 332.55(\delta x)^2$	$9.39(\delta x)$	2.84
HC	Height of column $= 25(\delta x)$ Characteristic length $\quad L = $ height/2 Radius of cross section $\quad R = 8(\delta x)$ $A = 1532.55(\delta x)^2$ Aspect ratio $= 3.125: 1$	$23.02(\delta x)$	2.36
BB	$A = 2660.43(\delta x)^2$ $R = 16(\delta x)$	$45.65(\delta x)$	3.45
SC	Radius $R = 6(\delta x)$ $A = 72(\delta x)^2$	$5.44(\delta x)$	5.70
CC	Height of column $H = 25(\delta x)$ Characteristic length $L = H/2$ Radius of HP cross section $\quad R_1 = 8(\delta x)$ Radius of caps $R_2 = 12(\delta x)$ $A = 2738.06(\delta x)^2$	$21.4(\delta x)$	12.30

FIG. 3. Arrangement of six hexagons, as in Fig. 1, to form broad branched plate. Star-shaped region enclosed by hexagons is filled with beads as part of crystal surface.

umn is viewed as a stack of hexagonal plates separated along the z axis by the grid spacing δz. Thus, a desired number of hexagonal plates with sides are stacked on top of each other, with $\alpha = 3$ and $\beta = 3$. The ratio of height of column to the side of a hexagonal face is chosen as desired to determine the stack size. In this paper, it was assumed to be $25\delta x$ over $8\delta x$, giving an aspect ratio of 3.125:1 (Table 1). Only α and β, the relative grid sizes are important for C, while Sh_0 is independent of actual dimensions.

c. Capped column

The capped column (CC) is modeled by adding two infinitesimally thin hexagonal plates of desired dimensions, one to the top and one to the bottom at a distance of δx from the hexagonal column, which is then modeled as above. In the present example, the added plates had side lengths of $12\delta x$ while that of the column cross section remained at $8\delta x$.

d. Broad branched plate

A broad branched plate (BB) is obtained by simply arranging a collection of hexagonal plates each of which is modeled as in section 4a; α and β are kept the same

as above, while the hexagonal plates are arranged as shown in Figure 3. As seen in the figure, the six hexagons are first arranged as shown. On the grid representation, a bead is then put on all the grids that are inside the hexagons as well as those grids that belong to the star-shaped region in the middle. This collection of beads represents the BB plate on our grid.

e. Stellar crystal

Modeling of a stellar crystal (SC) is markedly different from the others. It may be tempting to model the stellar crystal as six line segments intersecting at the center as seen in Fig. 4. However, when the algorithm is run a nonsensical value is obtained for Sh_0 with this particular representation because the central difference approximation (8) is inherently assuming that $\delta\mu$ in all three directions is larger than the width of the branches of stellar crystal (Fig. 4). This is not correct. A width of one lattice spacing needs to be given while the thickness is 0, as with BB.

5. Discrete version of Gauss's flux law

A simple method of numerically computing Sh_0 using the potential V obtained via Gauss–Seidel method requires computation of the capacitance C. Determination of C, in turn, is based on the computation of the net surface charge of the crystal that gives rise to the surface potential V_0. The total electric flux of the crystal is obtained by first enclosing the crystal in an inner virtual cage (as opposed to the outer Faraday cage with its zero
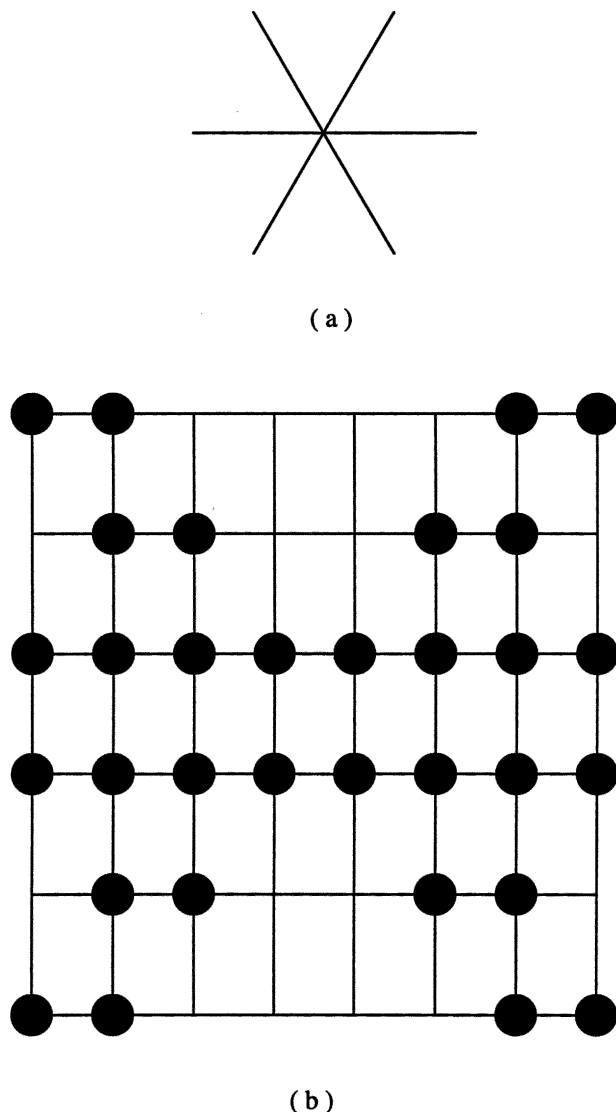
(a)

(b)

FIG. 4. (a) Inappropriate representation of stellar crystal; (b) approximation of a stellar crystal on *xy* plane. Branch width and length can be selected. Rotational symmetry of stellar crystal not exact in finite grid.
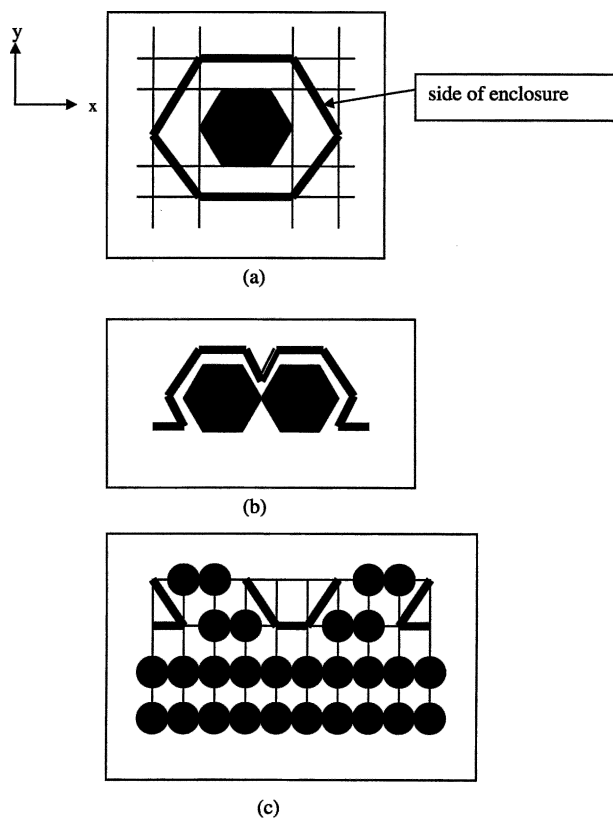

(a)

(b)

(c)

FIG. 5. Bird's eye view of enclosure shapes, indicated by thick line segments: (a) Hexagon enclosed by hexagonal column; top and bottom faces of column are one step along the *z* axis above and below the hexagon. (b) Enclosure for BB plate is a BB column with top and bottom faces one step along the *z* axis above and below BB plate. (c) Part of stellar crystal. An SC column enclosed the stellar crystal, with top and bottom faces one grid point along *z* axis away from SC plate. The distortions from ideal hexagons are as described in Fig. 2.

potential on the walls). The inner virtual cage is not a Faraday cage. That is, its walls are not assigned a constant potential or $V = 0$. It is simply a geometrical construct, a Gaussian surface through which the flux from the crystal is computed. It is positioned close to the test particle so that the divergence of the electrical field lines is greatest. The grid points lying on the walls of this inner cage inherit the potential V solved previously by the Gauss–Seidel method. The dimensions of the virtual cage depend on the crystal it encloses. But in all cases, the sides of this enclosure are at most two grid points away from the crystal (Fig. 5). The specific dimensions of enclosure for some of the shapes investi-

gated are also shown in Fig. 5. The best way to enclose a given shape is to simply mimic the outline of the crystal. For instance, an HP is enclosed by a hexagonal column whose sides are at most one grid point away from HP. An HC is enclosed by a larger HC and SC plate by a SC column. The CC is enclosed in two parts: the HC constituting CC is enclosed by a HC whose sides are just one cell away, while the two caps of CC are enclosed by HC like the way HC was described above. Each side of the inner cage consists of grid cells, which are called area elements. These cells have the same respective lattice spacing as the main grid. Approximation of the flux through a given area element whose outward unit normal is in $\pm\hat{\mu}$ direction is

$$F_{\pm\mu} = -\frac{V[(i, j, k) \pm \hat{\mu}] - V(i, j, k)}{\delta\mu}(\delta\nu)(\delta\gamma),$$

(12)

where ν and γ are the other two coordinates besides μ. In (12), (i, j, k) refers to the grid point at the center of the area element. This approximation may, a priori, seem coarse. However, as will be shown later, this approximation gives quite an accurate computation of Sh_0 for the dimensions investigated in this paper. The main reason for placing each side of the enclosure cage at most two lattice points away from its nearest side of the crystal is that such a construction allows for dealing only with $\partial V/\partial \mu$ rather than the three-component ∇V in computing the flux (due to the fact that the electric field is perpendicular to the surface of perfect conductors, the original crystals). Ideally, the enclosure cells should be at most one grid point away from the nearest surface of the crystal but it was found from numerical tests that extending out to two grid points away from the nearest surface of crystal has a negligible effect on the value of C and hence on the Sh_0. By using (12), $-\{V[(i, j, k) \pm \hat{\mu}] - V(i, j, k)\}/\delta\mu)$ is the value of the electric field perpendicular to the area element at (i, j, k). As the sides of the inner box move away from the crystal, the net flux, C, and thus the Sh_0 computed via (12), deviate from the results obtained with a closer inner box. As the Gaussian surface is enlarged and changed to different shapes, the flux through the surface deviated by an amount such that Sh_0 differed by no more than about 0.02. In accordance with Gauss's law, the net flux is invariant under change of the shape and size of the inner virtual cage, up to the minor numerical error mentioned above. The total flux through the inner cage is computed by summing the flux (12) through each of its area elements. From the net flux, the surface charge on the conductor is computed and its capacitance is established. Then Sh_0 is computed via (2) with δx carried throughout all of these calculations but canceling out at this last stage.

6. Dimensional analysis

At this point, a discussion on the physical length that $\delta\mu$ represents is warranted because when a flux through an area element is computed, α and β are not sufficient for expressing the net flux. Rather, the actual lattice spacing $\delta\mu$ is required. For example, a flux through a face whose unit normal is in $\pm\hat{z}$ direction is

$$F_{\pm z} = \delta x \left(\frac{\alpha}{\beta}\right)^{1/2} [-V(i, j, k \pm 1) + V(i, j, k)].$$

(13)

The only unknown value for the flux in (13) is the length scale δx, an actual physical length scale, which had not been discussed. After all, the Gauss–Seidel it-

eration (9) utilizes only the relative proportions α and β, while the potential V does not depend on the choice of δx. But (13) draws attention to δx. Note that $Q \sim \delta x$ is in electrostatic units, and so $C \sim \delta x$. Thus, via (1) we have $Sh_0 \sim (\delta x)^2/(\delta x)^2 = 1$; that is, although δx is unknown throughout our calculations, all δx cancel out at the end because the actual physical length scales are irrelevant in the computation of the dimensionless Sh_0. Only the relative proportions of shapes and boundary conditions are relevant.

7. Results and discussion

The uncertainties in the values of the molecular diffusion of heat and mass based on the approximations by Houghton (1950) and the measurements of McDonald (1963) led to the development of a numerical method, which allows the numerical calculation of these quantities by the solution of the controlling Laplace equation for an electrostatic analog. Examples of values for hexagonal plates, stellar and broad-branched crystals, prisms and capped columns have been obtained.

Applying the numerical method described above capacitance, C, and Sh_0 have been computed for crystal shapes of interest in cloud physics (Table 1). They are valid for geometrically similar shapes only. To allow some rough comparisons, the characteristic lengths were chosen either as the radius or half the column height. One word about the capped columns: its molecular transfer is highest because of the relatively large surface area and the exposure of the edges of the end plates.

Heat and mass transfer calculations and measurements are generally based on the assumption of the homogeneity of surface temperature (equivalent to constant electric potential in the electrostatic analogy). Deposition (and evaporation) of water molecules is diffusion controlled because the latent heat of deposition needs to be diffused away through the air. Higher deposition will lead to higher surface temperatures due to increased release of latent heat of deposition. This in turn translates into higher surface temperature and saturation vapor pressure at the surface and, consequently, a reduced concentration gradient. Hence, corrections would immediately be triggered and equilibrium will be maintained. This situation could only change if heat would be conducted away from hot spots at the crystal surface through the crystal interior. This does happen in hailstone growth (Zheng and List 1996), but is unlikely to be of any consequence in ice crystal growth because of the much smaller dimensions.

Once crystals assume a nonnegligible fall velocity, both heat and mass transfer will be increasing by the

addition of a Reynolds number-dependent convective part of Sh and Nu. The combined transfers have been measured by Schemenauer and List (1978) for the crystal types considered here. The transfers can now be properly anchored at Re = 0. This will be reported later with a full parameterization of the growth theory. Considering that free-fall experiments have been carried out for similar-shaped crystals by List and Schemenauer (1971), a combination with the heat and mass transfer is feasible, but only after the effect of oscillations, estimated at enhancing Sh by up to 20%, are understood. Then a combined experiment-based theory can be applied to ice crystals growing in the atmosphere and comparisons can be made to crystal growth in nature. Nevertheless, a first estimate indicates that molecular diffusion of mass and heat is dominant for crystals with diameters < 1 mm, that is, nearly all crystals occurring in the atmosphere.

Comparisons to Houghton (1950) and McDonald (1963) will not be made at this time because the shapes and aspects ratios treated are not similar. Nevertheless, it can be said that Houghton's approximations for hexagonal plates are within <5% of the new numerical values while McDonald's values are lower by up to ~50%. Thus, Houghton's approximations seem to be reliable for shapes obtained by compressing or stretching spheres. However, they are not useful for rectilinear-shaped crystals more complex than hexagonal plates. That is the realm of the newly developed scheme.

As mentioned before Chiruta and Wang (2003) carried out similar numerical studies with crystal shapes typical of rosettes. While their method of computation is similar in spirit to ours, they have used discrete curvilinear coordinates that would not be suitable for our rectilinear crystals. In turn, our rectilinear grid system is not suitable for studying their idealized rosettes, which they approximated by collections of rounded bullets. Because of the difference in our grid systems, the discrete versions of Gauss's law and Laplace equations are different. Chiruta and Wang (2003) have noted that when the ratio of grid box to particle size was greater than seven to one (as compared to eight to one in the present case), their numerical solutions were no longer sensitive to further changes in the size of the Faraday cage. This is similar to the present results when changing the size of the grid box from $150 \times 150 \times 150$ to $200 \times 200 \times 200$ produced differences in potential by at most 10^{-9} for grid points nearby the crystal faces.

In addition to establishing Sh_0 for better approxima-

tions of the hexagonal plate and different aspect ratios of columns, broad branched crystals, prisms and capped columns, the present work needs to be expanded to needles and particles of importance in cirrus such as bullets and rectilinear rosettes. Bullets can be simulated by tapering off a hexagonal prism at one end, rosettes could be thought of as assemblies of bullets. Such new numerical experiments on molecular diffusion would be of importance to both cloud physics and climate change models.

REFERENCES

Beard, K. V., and H. R. Pruppacher, 1971: A wind tunnel investigation of the rate of evaporation of small water drops falling at terminal velocity in air. *J. Atmos. Sci.,* **28,** 1455–1464.

Chiruta, M., and P. K. Wang, 2003: The capacitance of rosette ice crystals. *J. Atmos. Sci.,* **60,** 836–846.

Houghton, H. G., 1950: A preliminary quantitative analysis of precipitation mechanisms. *J. Meteor.,* **7,** 363–369.

Jayaweera, K. O. L. F., 1971: Calculations of ice crystal growth. *J. Atmos. Sci.,* **28,** 728–736.

List, R., and R. S. Schemenauer, 1971: Free-fall behavior of planar snow crystals, conical graupel and small hail. *J. Atmos. Sci.,* **28,** 110–115.

McDonald, J. E., 1963: Use of electrostatic analogy in studies of ice crystal growth. *Z. Agnew. Math. Phys.,* **14,** 610–619.

Pasternak, I. S., and W. H. Gauvin, 1960: Turbulent heat and mass transfer from stationary particles. *Can. J. Chem. Eng.,* **38,** 35–42.

Schemenauer, R. S., 1972: The convective mass transfer of snow crystal, conical graupel, and conical small hail models. Ph.D. thesis, University of Toronto, 146 pp.

——, and R. List, 1978: Measurements of the convective mass transfer of planar and columnar ice crystals. *Borovikov Memorial Issue,* Academy of Sciences of the USSR, 217–232.

Schuepp, P. H., and R. List, 1969: Mass transfer of rough hailstone models in flows of various turbulence levels. *J. Appl. Meteor.,* **8,** 254–263.

Strauss, W. A., 1992: *Partial Differential Equations: An Introduction.* John Wiley and Sons, 425 pp.

Todd, C., 1964: A system for computing ice phase hydrometeor development. Rep. ARG 64, Pa-121, Meteorology Research Inc., 30 pp.

Zheng, G., and R. List, 1996: Convective heat transfer of rotating spheres and spheroids with non-homogenous surface temperatures. *Int. J. Heat Mass Transfer,* **39,** 1815–1826.